Etoposide and olaparib polymer-coated nanoparticles within a bioadhesive sprayable hydrogel for post-surgical localised delivery to brain tumours

Phoebe McCrorie [a], Jatin Mistry [b], Vincenzo Taresco [b], Tatiana Lovato [b], Michael Fay [b], Ian Ward [c], Alison A. Ritchie [d], Philip A. Clarke [d], Stuart J. Smith [a], Maria Marlow [b,*,1], Ruman Rahman [a,*,1]

[a] Children's Brain Tumour Research Centre, Biodiscovery Institute, School of Medicine, University of Nottingham, NG7 2RD, UK
[b] Division of Advanced Materials and Healthcare Technologies, School of Pharmacy, University of Nottingham, NG7 2RD, UK
[c] School of Life Sciences Imaging, School of Life Sciences, University of Nottingham, NG7 2RD, UK
[d] Division of Cancer and Stem Cells, Faculty of Medicine and Health Sciences, University of Nottingham, NG7 2RD, UK

ARTICLE INFO

ABSTRACT

Glioblastoma is a malignant brain tumour with a median survival of 14.6 months from diagnosis. Despite maximal surgical resection and concurrent chemoradiotherapy, reoccurrence is inevitable. To try combating the disease at a stage of low residual tumour burden immediately post-surgery, we propose a localised drug delivery system comprising of a spray device, bioadhesive hydrogel (pectin) and drug nanocrystals coated with polylactic acid-polyethylene glycol (NCPPs), to be administered directly into brain parenchyma adjacent to the surgical cavity. We have repurposed pectin for use within the brain, showing *in vitro* and *in vivo* biocompatibility, bio-adhesion to mammalian brain and gelling at physiological brain calcium concentrations. Etoposide and ola-parib NCPPs with high drug loading have shown *in vitro* stability and drug release over 120 h. Pluronic F127 stabilised NCPPs to ensure successful spraying, as determined by dynamic light scattering and transmission electron microscopy. Successful delivery of Cy5-labelled NCPPs was demonstrated in a large *ex vivo* mammalian brain, with NCPP present in the tissue surrounding the resection cavity. Our data collectively demonstrates the pre-clinical development of a novel localised delivery device based on a sprayable hydrogel containing thera-peutic NCPPs, amenable for translation to intracranial surgical resection models for the treatment of malignant brain tumours.

1. Introduction

Glioblastoma Multiforme (GBM) is a World Health Organisation grade IV brain tumour with a dismal 14.6-month average survival [1] from diagnosis when patients receive the standard-of-care therapy. This comprises of maximal safe surgical resection followed by concurrent chemoradiotherapy. Temozolomide (TMZ) is the chemotherapy of choice determined by the Stupp protocol [2,3], due to its efficacy against GBM, increasing survival times from 12 months (radiotherapy alone) to 14.6 months [3]; however, the efficacy of TMZ is limited to tumours with the O-6-methylguanine-DNA-methyltransferase (MGMT) gene promoter methylated. Silencing of the MGMT promoter by methylation leads to reduced DNA repair, thus rendering TMZ associated DNA damage more efficacious [4].

Despite vast amounts of research, the average lifespan of a patient diagnosed with GBM has not greatly increased over the years [5,6]. The efficacy of systemic chemotherapy is limited in considerable part due to the blood brain barrier (BBB), a physiological obstacle which restricts molecular therapeutics from being delivered at efficacious concentrations within the microenvironment of residual post-surgical neoplastic cells. This has led to considerable research focus into localised drug delivery [7,8] and repurposing systemically toxic chemotherapies [9]. Moreover, nanotechnology has advanced the field of local drug delivery, whereby drugs are encapsulated within a nano-sized carrier to protect the chemotherapeutics from rapid degradation within the body, and in turn, to protect the brain from drug-associated toxicities. This capability for increased half-life of the drug, has enhanced the efficacy of many drugs [10].

For the delivery of chemotherapeutics targeting residual cells remaining post-surgery, the nanoparticles (NPs) ideally need to diffuse through the brain parenchyma, therefore transporting the drug further from the administration site than by drug molecule diffusion alone. Recent work has explored the effect of NP size on the ability to penetrate through brain tissue. One study in mice showed that 40 and 100 nm polystyrene (PS) NPs with a dense poly-(ethylene glycol) (PEG) layer, rapidly diffused throughout the brain tissue, whereas 200 nm PS-PEG NPs did not, when following their fluorescent signals post-intracranial injection. Further work showed that these NPs at 114 nm in diameter were able to rapidly diffuse through brain tissue [11] and 70 nm poly (lactide-co-glycolide) (PLGA)-PEG NPs (encapsulating paclitaxel), were able to diffuse 100-fold faster than analogously sized paclitaxel-loaded PLGA NPs without a PEG coating [12].

For this work, etoposide and olaparib nanocrystals were chosen for coating with polylactic acid-polyethylene glycol (PLA-PEG) to create **n**anocrystals **c**oated with **PLA-PEG** (NCPPs). These chemotherapeutics were chosen due to previous work in the group showing efficacy against GBM *in vivo* [13,14]. Etoposide functions by forming a ternary complex with DNA and the Topoisomerase II enzyme, which prevents re-ligation of the DNA strands, thus causing the strands to break, leading to cell death [15]. Whereas olaparib is a poly-ADP ribose polymerase (PARP) inhibitor, targeting the PARP enzyme involved in DNA repair. As cancer cells rely on this enzyme to catalyse rapid cell division, PARP inhibition renders cells more susceptible to DNA damage-induced apoptosis [16]; there is also ongoing work to study the radiosensitising ability of the drug [17,18].

The method used to encapsulate drugs in this study is a novel approach whereby a drug 'nano-crystal' is formed, which is later coated with a polymer layer, generating high drug loaded NPs [19]. The process of NP materialisation occurs when the concentration of the molecule in solution exceeds that which is soluble; therefore, the molecules nucleate, forming small NPs. Following nucleation, the particles grow by a process called Ostwald Ripening, whereby smaller, less stable particles resolubilise and attach onto the surface of larger particles, which then coagulate and coalesce [20]. This drug 'nano-crystal' can be coated with a polymer coating to provide a steric barrier, protecting them from aggregating, reducing further increase in NP size and thus increasing colloidal stability. This method has been previously reported to coat many metal-based NPs [21]. The amphiphilic polymer coating was added to these NPs to transfer these hydrophobically capped metal nanocrystals from an organic to an aqueous environments and to reduce aggregation of the NPs [22,23]. Our study used a PLA-PEG based polymer, which was chosen due to the similarity to the formulation used for Genexol®, which is approved for use in South Korea. Genexol® uses the same polymeric backbone, selected due to the non-immunogenic properties of PEG and the biodegradable core-forming PLA [24]. Since this was approved, many studies have trialled PLA-PEG NPs *in vivo* and demonstrated biocompatibility [25–27].

Just as the NPs described above, many studies have used hydrogels or polymers to deliver chemotherapeutics to the target cells [28]. However, to date, the only local drug delivery system (DDS) for brain tumours which is approved for human use is the Gliadel® Wafer. The wafers, loaded with carmustine [29], have significantly increased the lifespan of patients by an average of 3.6 months when compared to TMZ alone (10 combined trials, n = 379 patients; median survival range 12.7–21.3 months) [30]. However, these wafers are rigid and do not conform to the irregular-shaped surgical cavity walls. This leaves gaps between the wafers and brain tissue, reducing effective drug delivery [31]. To address this issue, it is hypothesised that a bioadhesive hydrogel could prevent wash-away of NPs by the interstitial fluid by holding them temporarily in place before the NPs diffuse away. Similar drug-loaded bioadhesive hydrogels have been demonstrated in a wide range of applications [32–34]. Delivery of this hydrogel via a spray device should allow superior conformation to the cavity walls.

The bioadhesive gel of choice is low methoxyl (LM) pectin. Pectin, from citrus fruit peel, is made up of 1–4 linked α-D galacturonic acid residues (with varying degrees of methyl esterification (DE)) with a small fraction of rhamnose and small side chains from other sugars such as L-arabinofuranose and D-galactopyranose [35,36]. Pectin is defined as LM when the (DE) is below 50% and these pectin grades tend to form gels electrostatically stabilised by divalent ions (e.g. calcium) or other cationic species. As a result, pectin remains in solution state until it comes into contact with calcium, at which point it forms a gel via the 'egg-box model'; one calcium ion can bond with two carboxyl groups on two different chains [37], forming an ionic cross-linked gel.

The brain has an extracellular calcium concentration of between 1.5 and 2.0 mM [38] and hence, it is predicted that the pectin will form a gel structure upon contact with brain tissue. Pectin is used in other applications *in vivo*, such as to deliver drugs nasally for breakthrough pain in cancer patients [39]. In the past, it has also been trialled as a plasma expander for World War 2 [40], with one report stating that no weight loss or toxicity was observed in 776 animals when injected with pectin every other day for six weeks [41]; therefore we propose its functionality and biocompatibility will be ideal for this application.

In this work we have developed a novel DDS, which comprises of highly drug-loaded (etoposide and olaparib) polymeric NCPPs, held within a bioadhesive gel and delivered to brain parenchyma adjacent to the surgical resection cavity using a spray device. To our knowledge, this is the first-time pectin has been delivered to the *in vivo* brain, and it is the first time a spray device has been used to deliver drug-loaded polymeric NPs to a surgical resection margin within the brain. We hypothesise that this novel DDS will generate a new means of drug delivery into surgical resections of GBM and potentially aid increased survival times with further research.

2. Materials

Materials were purchased from the following: poly(ethylene glycol) methyl ether, Mn = 5000; Pluronic F127 (PF127) and hydroxypropyl-β-cyclodextrin (HPβCD), (Sigma-Aldrich); DL-LA, 99% (Fisher Scientific); artificial cerebrospinal fluid (aCSF; Tocris); etoposide and olaparib (ApexBio); erlotinib (SelleckChem); Cyanine5 amine (Cy5; Lumiprobe Life Science Solutions); RealTime-Glo^TM MT cell viability assay (Invitrogen); AccuGENE® 10 × PBS buffer (VWR); 50–100 μL classic line spray devices (horizontal spray) were kindly donated by Aptar Pharma, Germany. Low methyl-esterified citrus fruit pectin, P101, P102, P104 and P105 were kindly donated by CP Kelco, Denmark.

3. Methods

3.1. In vitro biocompatibility analysis

3.1.1. Pectin

All gels were made in sterile conditions. Briefly, 1 M calcium chloride was aliquoted into a 96-well plate and frozen at −20 °C overnight. Pectin powder was weighed into a glass vial and PBS was added drop wise whilst stirring on a heated magnetic stirrer (Technico) at 70 °C. Once solubilised, the pectin was transferred onto the frozen calcium and the plate left at 37 °C overnight to form gels before washing 3x with PBS. Gels were made at 50, 100 and 200 μM. For solution state assays, the pectin was not mixed with calcium. For astrocytes (#1800, ScienCell), the washed pectin gels were incubated in 100 μL astrocyte medium for 24 h and the medium then transferred onto cells. These cells were indirectly cultured with pectin due to issues with co-culture. If gels sit directly on top of the cells, they can reduce nutrient flow from the medium to the cells [42]. In addition, they also can remove cells from the well when the hydrogel is removed [43]. This resulted in reduced viable astrocyte numbers (data not shown); therefore, it was determined that indirect culture (i.e. transfer of medium first incubated with gels, into cell plates) would show if leached pectin by-products could cause toxicities. This method has also been adopted by others culturing sensitive

astrocytes with hydrogels; for example, Tate et al. indirectly cultured rat astrocytes with methylcellulose-based constructs, with positive results [44]. This method was not utilised for U87 cells (discussed below) as these cells are not as sensitive to culture as primary human astrocytes; therefore, no contact inhibition was seen for U87 cells. For astrocytes, the gels were incubated with medium for 24 h to ensure that there was enough time for leaching of pectin into the medium, allowing for more comparable results.

Human astrocytes were cultured as per ScienCell guidelines at a seeding density of 5000 cells/cm^2. Cell viability post-pectin incubation was measured using a RealTime-Glo^{TM} MT cell viability assay as per manufacturer guidelines. Viability was measured via luminescence using a Fluostar Omega plate reader (BMG Labtech) at 24, 48 and 72 h post pectin medium addition.

U87 GBM cells (ATCC®) were cultured in DMEM supplemented with 10% FBS (Gibco, v/v) and 1% Penicillin/Streptomycin, incubated at 37 °C with 5% CO_2 and passaged upon reaching sub-confluency. Following seeding at 5000 cells/well in a 96 well plate, the solution state or gel state pectin was added after 24 h. Cellular viability was assessed using a PrestoBlue™ assay as per manufacturer guidelines. Following incubation with cells, PrestoBlue™ was transferred into a black 96-well plate and fluorescence measured using a Fluostar Omega plate reader (BMG Labtech) at λ_{Ex} 544 nm and λ_{Em} 590 nm.

3.1.2. Polymer-only nanoparticle biocompatibility

Polymer-only NPs were made in sterile conditions. Briefly, mPEG$_{5000}$-PLA$_{100}$ polymer was dissolved in 1 mL acetone and added dropwise to 5 mL PBS, stirring at 550 rpm. Samples were left stirring overnight for solvent evaporation. NPs were filtered through a 0.22 μm Millex-GV filter and added to astrocytes at a final concentration of 0.0625 – 1 mg/mL. Viability was measured at 72 h using a PrestoBlue™ assay.

3.2. In vitro pectin degradation

8 mg gels were incubated in aCSF for up to 28 days at 37 °C. At each time point, the supernatant was collected and filtered through a Millex 4 mm, 0.45 μM filter (Sigma Aldrich), before running on Gel Permeation Chromatography (GPC). The remaining gel was freeze dried and weighed. GPC of the supernatant was carried out using a Wyatt dawn 8 + 1200 Infinity series in a system equipped with a Polymer Labs aquagel-OH guard column (50 × 7.5 mm, 8 μm) followed by a PL aquagel-OH MIXED-H analytical column. Standard Dulbecco's Phosphate Buffered Saline (DPBS) was used as the mobile phase, with a flow rate of 1 mL/min. Molecular weight (Mw) was calculated using a Wyatt DAWN® HELEOS® II MALS, using a dn/dc of 0.125 mL/g. The resulting chromatograms were analysed using ASTRA® software, V.6.1.2.84 (Wyatt Tech Corp).

3.3. Bioadhesion study

Fresh 50 μm rat brain tissue slices were attached to a 20 mm probe (top) of a TA-XT plus texture analyser (Stable Micro Systems, UK) using double-sided tape. A 200 μM pectin gel was placed onto the stage and 0.5 N of force applied by the probe for 60 s before lifting at a speed of 0.5 mm/sec until reaching a height of 10 mm, recording the force required to detach the two surfaces. A control sample was used where no brain slice was attached to the top probe.

3.4. Gelling concentration of pectin

Adapted from Castile et al. [39], solubilised 200 μM pectin and Fast green FCF dye was placed into a 3 mL spray bottle with a 50 μL actuator and sprayed perpendicularly from 1 cm distance onto a 45° angled TLC plate which had been soaked for 10 min in 1.5 mM calcium chloride. Once sprayed, the plate was left for 5 min before drip length was measured.

3.5. Polymer synthesis

mPEG$_{5000}$-PLA$_{100}$ was synthesised and characterised as per methods reported by Phan et al. [45] via PEG-initiated ring-opening polymerization of lactide block copolymer. Briefly, the desired amount of LA (6.94 mmol) and mPEG$_{5000}$-initiator (0.0694 mmol) were weighed into a vial (pre-dried in an oven at 100 °C). The [M]:[I] ratio was kept fixed at 100:1. mPEG$_{5000}$ and LA were dissolved in 10 mL of dichloromethane in a capped vial and the mixture was allowed to fully dissolve at room temperature. 1,8-Diazabicyclo[5.4.0]undec-7-ene (Sigma-Aldrich) was then added at 2% (w/w, compared to the monomer; 0.13 mmol), to initiate the ring opening polymerization. After 20 min of reaction time the polymer was purified via multi-precipitation steps (cold hexane: diethyl ether mixture) and dried in a vacuum oven at room temperature (25 °C) with quantitative conversion of monomer into polymer (from 80 to 98%).

3.6. Labelling of mPEG$_{5000}$-PLA$_{100}$ with Cy5

Cy5 was chemically attached to the hydroxyl-terminus of the polymers via disuccinimidyl carbonate (DSC, Sigma-Aldrich) coupling [46]. 100 mg of polymer (0.005 mmol), 10 μL triethylamine (TEA, 0.07 mmol) in 0.5 mL dry acetonitrile (MeCN) and DSC (0.019 mmol) in 1 mL dry MeCN was added to a dry glass vial under continuous stirring at 0 °C and left for 3 h. A stock solution of Cy5-amine (0.002 mmol) and TEA (0.07 mmol) was prepared in dry MeCN, with Cy5 at 1% (w/w) to the polymer and the TEA concentration in excess with respect to the dye. Subsequently, 1 mg Cy5 and 10 μL TEA were dissolved in 2 mL dry MeCN. This was then added to the reaction under constant stirring at 0 °C and left for a further 3 h. Finally, the resultant conjugated mPEG$_{5000}$-PLA$_{100}$-Cy5 was purified through multiple precipitation steps in cold hexane: diethyl ether mixture. Coupled-Cy5 content was evaluated against Cy5-amine standard calibration curve using fluorescence (λ_{ex} = 647 nm, λ_{em} = 665 nm).

3.7. Nanoparticle manufacture

Nanocrystals **c**oated with m**P**EG$_{5000}$-**P**LA$_{100}$ (NCPPs) were prepared by a modified method from Styliari et al. [19]. Briefly, 1.25 mg etoposide or olaparib were dissolved in 1 mL solvent (acetone, and acetone: MeCN:MeOH [1:1:1], respectively) before adding dropwise into 5 mL aqueous phase, stirring at 550 rpm. Drug-only nanocrystals were left stirring overnight to allow solvent evaporation, before mPEG$_{5000}$-PLA$_{100}$ dissolved in 1 mL acetone was added dropwise into the drug nanocrystal aqueous phase whilst stirring. Samples were left stirring overnight to allow solvent evaporation before free drug was removed by centrifugation at 10000 × g for 5 min at room temperature (Eppendorf centrifuge 5430, Germany). NCPPs were then concentrated with gaseous N_2 to a predetermined volume and centrifuged again. Polymer-only NPs were generated by dissolving polymer in acetone and adding dropwise into aqueous phase stirring at 550 rpm. Samples were left overnight for solvent evaporation.

3.8. Transmission electron microscopy (TEM)

NP structure was analysed by depositing samples onto a graphene oxide on Holey Copper 300 mesh (EMResolutions) and analysed using a JEOL 2100F TEM operating at 80 kV, equipped with a Gatan Orius CCD.

3.9. Dynamic light scattering (DLS)

The diameter (d.nm), polydispersity index (PDI) and zeta potential of NPs were determined using a Zetasizer Nano ZS (Malvern Instruments Ltd.). A NP dispersion was diluted in Milli-Q water at intensity in the

range 10^4–10^6 counts/sec and measurements were performed at 25 °C on a 173° backscatter angle. Results are reported as the mean of three independent measurements of three different batches (n = 9) ± standard error of the mean (SEM). For Zeta potential analysis, NPs were suspended in 10 mM NaCl.

3.10. NCPP stability

To determine NCPP stability in different conditions, 0.3 mg/mL NCPPs were incubated at a 1:1 ratio with DMEM, aCSF and PBS (n = 3). The samples were incubated at 37 °C and size measurements of the samples were conducted by DLS as previously described above after 1 and 24 h.

3.11. Drug loading and drug release

Drug loading of 1 mg freeze-dried NCPPs was analysed using high-performance liquid chromatography (HPLC) (UltiMate 3000, Thermo-Fisher). A full validation of the HPLC methods was performed in accordance with the FDA Guidance for Bioanalytical Method Validation [47]. Separation of compounds was achieved on an ACE 5 C_{18} column (250 × 4.6 mm plus an ACE 5 C_{18} 10 × 3 mm guard column) heated at 40 °C. For olaparib, the mobile phase consisted of (10 mM) pH 4 ammonium acetate/acetonitrile (55/45 v/v) at 1 mL/min for 10 min and effluent was monitored at 254 nm [48]. Erlotinib was used as an internal standard (IS) at 20 µg/mL and quantitation was achieved by measurement of the peak area ratios of olaparib to erlotinib compared to a calibration curve. The IS was added to samples in equal amounts and therefore corrects for variations in the analyte response caused by variability in the sample preparation and analytical procedure; thus it allows for more accurate quantification of drug in the sample [49].

For etoposide, the mobile phase consisted of (0.5 mM) pH 3.5 formic acid/Acetonitrile (65/35 v/v) at 1 mL/min for 10 min and effluent was monitored at 220 nm [50]. Erlotinib was used as an IS at 10 µg/mL and quantitation was achieved by measurement of the peak area ratios of etoposide to erlotinib. Two high, medium and low quality control samples were included to check the accuracy of the calibration curve. Drug loading was calculated as follows:

$$\% \ drug \ loading = \frac{amount \ of \ coated \ drug \ (\text{mg})}{mass \ of \ NP \ (\text{mg})} \times 100$$

For drug release, 500 µL concentrated NCPP suspension (±200 µM pectin) was added to a 0.5 mL, 3.5 MWCO, slide-a-lyzer cassette containing 14 mL, 10% (w/v) HPβCD and incubated at 37 °C. 10% HPβCD was chosen due to previous studies reporting solubility of both etoposide and olaparib [51,52]. 2 mL samples were taken and replaced (to maintain sink conditions) at 0, 0.08, 0.5, 1, 2, 4, 6, 24, 48, 72 and 120 h. Samples were filtered through a 0.22 µm Millex-GV filter before running on HPLC.

3.12. Spraying the formulation

NCPPs at ~0.3 mg/mL in water or PBS as the aqueous phase ±0.5% HPβCD (w/v) or 0.5% PF127 (w/v), were added to a 5 mL glass Aptar Pharma spray bottle (50 µL actuator). Once sufficiently primed, samples were sprayed and collected in an Eppendorf, where they were sized using DLS as described above, and compared to a pre-spray control. The surfactant/sugar was trialled with the formulation to aid stability of the NPs against the shear stress of the spray device.

3.13. Cy5-labelling of pectin

100 mg Pectin 101 was dissolved in 10 mL of pure water (1% w/v) and allowed to completely solubilize at room temperature under continuous stirring. 0.02 mmol Cy5 (2% mol/mol, compared to pectin) was dissolved in 1 mL of pure water and added to the cloudy solution of pectin. The amount of dye was added to couple approximately 5% of the free carboxylic groups alongside the main pectin backbone. Finally, 3 mL of an aqueous solution of 1-Ethyl-3-(3-dimethylaminopropyl)carbodiimide (0.30 mmol, Sigma-Aldrich) was added dropwise to the pectin-dye solution. The EDC/Cy5 final molar ratio selected was approximately 15/1. To the final solution, a catalytic amount of 4-Dimethylaminopyridine was added and the reaction left to stir for 48 h and dialysed against pure water for 2 days.

3.14. In vivo biocompatibility

7 male CD-1 NuNu mice (10–11 weeks) were purchased from Charles River, UK. The experiment was conducted under the UK Home Office Licence number PPL P435A9CF8. LASA good practice guidelines, FELASA working group on pain and distress guidelines and ARRIVE reporting guidelines were also followed. Mice were maintained in Individually Ventilated Cages (IVCs) (Tecniplast, UK) within a barriered unit illuminated by fluorescent lights set to give a 12 h light–dark cycle (on 07.00, off 19.00), as recommended in the United Kingdom Home Office Animals (Scientific Procedures) Act 1986. Following a week of acclimatisation, the mice were randomly allocated into study groups of 1 control mouse and 6 experimental mice to receive 200 µM, 3% Cy5-labelled pectin (w/w). While under general anaesthesia, a small incision was made through the skin along the midline of the skull. The mouse was secured onto an electronic stereotaxic frame (Harvard Apparatus UK) using a nose clamp, and a small burr-hole was drilled through the skull, (1 mm to the right of the midline, 1.5 mm anterior to the lamboidal suture and 2 mm deep), using a 0.7 mm diameter surgical drill bit. A larger drill bit was then used to enlarge the burr hole to approximately 1–2 mm. The labelled pectin was then dripped into the hole via a pipette and left for one minute, after which time the excess was removed with a cotton bud and the process repeated to get the maximum volume into the hole. In order to add a larger volume of pectin, healthy brain would have had to be removed. The burr hole was then plugged with bone wax and the skin sutured shut. The control mouse underwent the same surgery without receiving the pectin to confirm the procedure itself did not produce (auto)fluorescence. 24 h after surgery, the animals were again anaesthetised and imaged. Three mice were culled by cervical dislocation and the brains and skulls were dissected out and imaged *ex vivo* (Group 1). Imaging was repeated in the remaining mice at 7 days and 14 days (Group 2 plus control). All images were collected using the IVIS® Spectrum imaging system, PerkinElmer (MA, USA) and analysed using the Living Image software.

3.15. Haematoxylin and eosin staining

Mouse brains were fixed in 4% paraformaldehyde and 4 µm sections obtained in a series from the surgical boundary. Briefly, sections were baked at 60 °C overnight and then deparaffinised by submerging the slide in xylene three times for 10 min. Slides were treated sequentially in 100, 95, 80, 70% ethanol, water, Harris haematoxylin and eosin (Surgipath, UK). Stained sections were rehydrated, mounted with DPX mounting medium and then observed by light microscopy.

3.16. Ex vivo analysis of the DDS

0.3 mg/mL Cy5-labelled polymer-only NPs (to match the final concentration of concentrated NCPPs following N_2 concentration) were sized using a Viscotec and then added to pectin powder to make a 200 µM solution; 5% PF127 in 0.1 M PBS was then added so that the final concentration was 0.5% PF127 and 0.01 M PBS in the formulation. Once solubilised via stirring, the sample was added to a 5 mL glass Aptar Pharma spray bottle (50 µL actuator) and primed. Ten sprays were administered to a 1 cm^3 cavity within a fresh porcine cadaver brain before sequential biopsies were taken from below the cavity by a neurosurgeon. Biopsies were snap frozen and cryosectioned (CM3050 S,

Leica, Germany) before analysis using a Zeiss LSM880C Confocal Microscope.

4. Results & discussion

To determine whether the DDS was suitable for delivery of chemotherapeutics for GBM, a hydrogel was trialled for biocompatibility and degradation *in vitro* and *in vivo*, followed by the development and characterisation of drug loaded NPs. These components were tested with the commercial spray device and ultimately, trialled in a large *ex vivo* mammalian brain.

4.1. Pectin degradation in vitro

The use of a hydrogel in the DDS is hypothesised to prevent the NPs being washed away via interstitial fluid and the CSF. However, the degradation of pectin within the brain is paramount to allow for elimination from the brain to reduce any associated side effects. Preliminary *in vitro* tests were conducted to observe if there was any degradation of the gels. Pectin gels (200 μM) were incubated in aCSF at 37 °C and the supernatant collected at various time points and assessed using GPC to establish if any pectin had degraded into lower molecular weight polymer chains or oligomers.
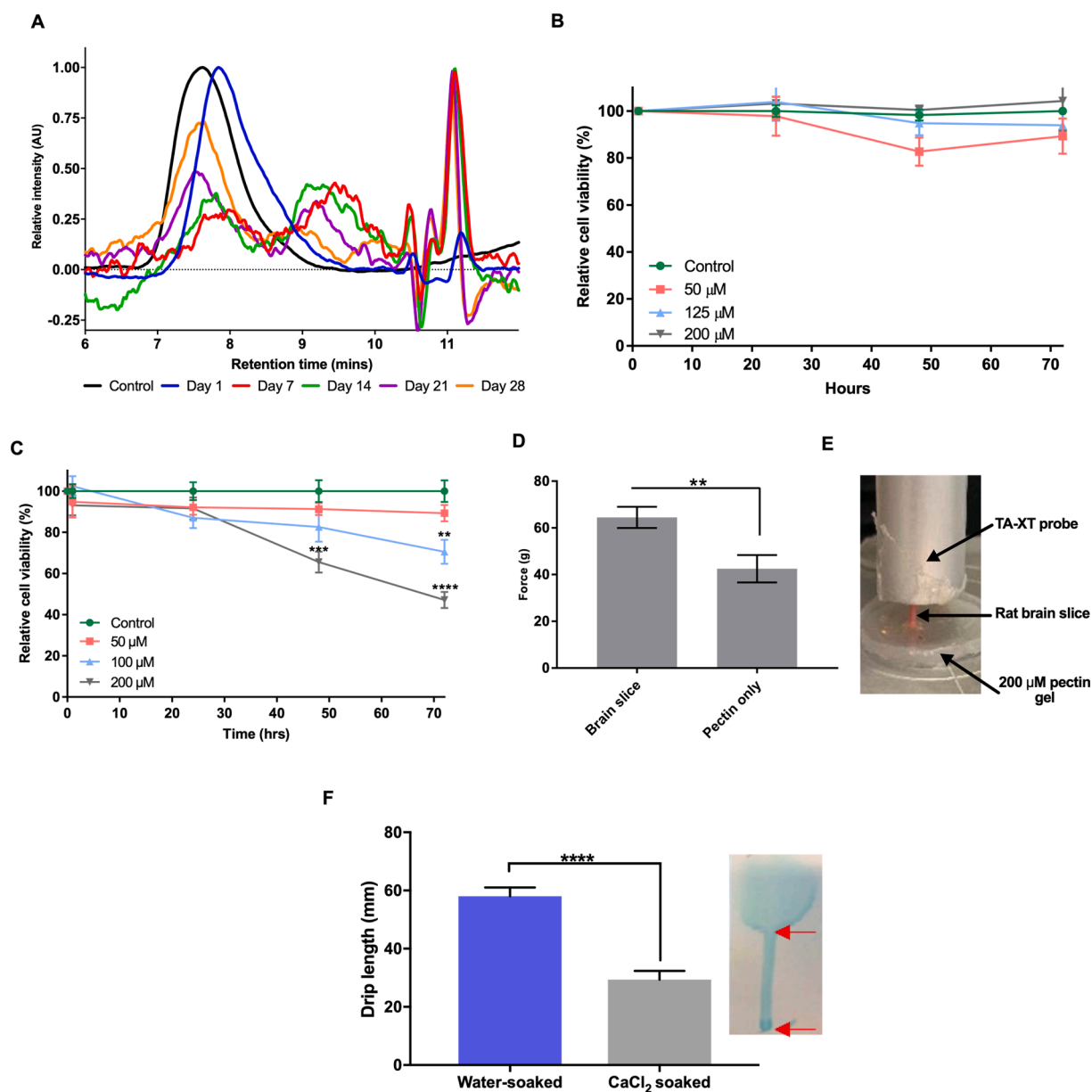
Fig. 1. **Brain biocompatibility of pectin hydrogel *in vitro*.** (A) Pectin GPC chromatograms following incubation in excess artificial CSF from 1 to 28 days, $n = 3$. (B) U87 cell viability measured using a PrestoBlue™ assay when cells were incubated with 50 μM–200 μM pectin gels at 24 to 72 h, with no significant difference observed using a one-way ANOVA with a Dunnett's post-hoc test when compared to the control, P > 0.05. Results are displayed as mean ± SEM, $n = 9$. (C) Human astrocyte cell viability measured using a RealTime-Glo™ assay when cells were indirectly incubated with 50–200 μM pectin from 1 to 72 h. Results are displayed as mean ± SEM, $n = 9$, with significant reduction in viability determined using a one-way ANOVA with Dunnett's post-hoc test. (D) Force required on a TA-XT texture analyser to remove a rat brain slice from a 200 μM pectin gel, with results displayed as mean ± SD, $n = 4$. (E) Corresponding image showing bioadhesion of the rat brain slice to the pectin gel. (F) Drip lengths of a 200 μM pectin solution sprayed onto TLC plates soaked in d·H₂O control or 1.5 mM CaCl₂. TLC plates were fixed at a 45° angle and the drip length was measured as indicated by the red arrows in the inset image. Results are displayed as mean ± SEM, $n = 6$, with a significant reduction in drip length determined using a one-way ANOVA with Dunnett's post-hoc test. **** = P < 0.0001. (For interpretation of the references to colour in this figure legend, the reader is referred to the web version of this article.)

Fig. 1A shows that the longer the gels were incubated with aCSF, the later the pectin eluted from the column, demonstrating a time-dependant degradation. Fig. Supplementary Fig. S1 shows the corresponding molecular weights for the peaks in the GPC chromatograms, which reveal that over time, the pectin reduced in molecular weight to approximately 1.4% of its original weight. Over this period, the 7.9 ± 0.4 mg gels (mean $\pm$ SD, $n = 18$, freeze-dried weight) lost 2.5 ± 0.8 mg, also indicating degradation in aCSF. This degradation could be a result of the hydrolysis of the cross-linked pectin gel mass into shorter chains by the PBS and temperature of incubation [53], hence the reduction seen in the Mw from GPC analysis. However, the range of the GPC column used is 6000 to 10,000,000 Da. Therefore, the values in Supplementary Fig. 1, from day 7 onwards are not reliable, accurate values. Nevertheless, these results show that the pectin found within the aCSF had considerably degraded from the initial size of 196 kDa within the first 7 days of incubation.

It has been reported that natural polyuronates such as pectin and alginates are quite resistant and slow to degradation [54]; therefore, many studies have investigated enzyme cleavable modifications to the pectin chains. One laboratory has developed matrix metalloproteinase-cleavable norborene cross-linked pectin gels, which were degraded over 9 h in the presence of collagenase type 2 as a function of cross-linker density. The authors hypothesised that the cleavage of the cross linkers, separating the gel into soluble pectin chains, make them more susceptible to the proteolytic environment in vivo. Similarly, Munarin et al. generated pectin and RGD-pectin microspheres at 1 g/mL which degraded slowly over 24 h in PBS, with the RGD-pectin degrading quicker than the non-RGD equivalent [55]. In vivo, it has been shown that subcutaneous pectin gels in mice had begun to degrade after one week, showing severe fragmentation at 1.5% (w/v) and slight fragmentation at 2.5% (w/v) [56]. Collectively, these studies and our data, give promise that the pectin should degrade, albeit slowly, in an in vivo environment.

4.2. In vitro biocompatibility of pectin

Initially four pectin grades were trialled for use with the DDS; as shown in Fig. Supplementary Fig. S2, each grade differs by the degree of esterification (DE) and hence their calcium reactivity. Exposure to pectin 102 and 104 resulted in a reduction in U87 cell viability (chosen for preliminary screening, U87 is a robust GBM cell line, therefore any reduction of cell viability in this cell line is likely to predict much greater sensitivity in healthy cells such as primary human astrocytes) at various time points in solution and gel state, likely linked to calcium reactivity and the ability of pectin to sequester calcium from the cell medium. McKay et al. have investigated the ability of in situ calcium responsive hydrogels made of alginate and chitosan to remove calcium from areas following acute spinal cord injury (SCI), due to the ability of these hydrogels to sequester calcium, which is increased following SCI. They found that the elastic modulus of the gel was very sensitive to mM changes in calcium concentration, demonstrating an ability to sequester calcium ions [57]; thus giving credibility to the theory that high reactive pectin gels could be removing vital calcium from the cells.

Pectin 101 was chosen over pectin 105; although both were biocompatible, pectin 101 had a slightly lower DE, which is more calcium reactive and thus appropriate given the low endogenous calcium levels within the brain. In vitro biocompatibility analysis of pectin 101 showed no toxicity in the U87 GBM cell line over 72 h when exposed to 50 – 200 μM pectin gels (Fig. 1B); however, it did show a concentration dependent reduction in human astrocyte metabolic activity when indirectly cultured in pectin medium (Fig. 1C). Astrocytes are the most abundant glial cell found within the human brain and were therefore chosen to represent 'healthy' brain cells. Astrocytes are involved in several functions including supporting an intact BBB, regulating water and ion homeostasis, in addition to roles within tripartite synapses [58].

Following 72 h, the astrocyte viability was 90, 70 and 47% for 50,

100 and 200 μM pectin concentrations, respectively. Primary astrocytes are more sensitive in culture than GBM cell lines [59]. In addition, pectin is an anionic polysaccharide with a pKa around 3.5); therefore, pectin and its oligomers may reduce the pH of the media, accounting for the decrease in cell viability. Goldman et al. found that neurons and glia in vitro were sensitive to short incubation times with lactic acid and hydrochloric acid, with 1 h incubations in pH 5.2 lactic acid resulting in cell death [60]. Hansen et al. similarly found longer exposure times to acid, reduced astrocyte cell viability in vitro [61]. This reduction in astrocyte viability could also be as a result of the calcium sequestration of pectin, as described above. However, due to homeostatic mechanisms in vivo, it was assumed that pH and calcium changes due to pectin would be reduced in vivo, justifying the continuation of pectin within the DDS.

4.3. Bioadhesion of pectin gels to brain tissue

Pectin hydrogels need to be able to adhere to brain tissue in order to prevent wash-off of the NPs. Many previous studies have explored the bioadhesion of hydrogels to animal tissue by means of a TA-XT texture analyser, which analyses the force required to separate two materials from one another. In our study, pectin gel bioadhesion to rat brain slices showed that when a 0.5 N force for 60 s was applied, there was a significant increase in force required to detach the gel from the rat brain slice, relative to when no brain slice was present (Fig. 1D).

The image in Fig. 1E shows the brain attached to the pectin gel as the probe moves away. This data demonstrates that when the pectin is sprayed into the brain, the gel has the potential to adhere due to the bioadhesive forces, instead of being washed away by the interstitial fluid. Wattanakorn et al. also studied the bioadhesive nature of low DE versus high DE pectin discs on porcine buccal tissue, demonstrating that low DE pectin has superior bioadhesive properties; they attributed this to the higher hydrophilicity of low DE pectins [62], which has also been shown with other hydrophilic polymers in a different study [63]. Increased hydrophilicity allows for more hydrogen bonds between tissue and pectin gels. Thirawong et al. showed that a higher pH (4.8 versus 1.2) gave superior adhesion of pectin to gastrointestinal mucosa and Markov et al. demonstrated that higher concentrations of pectin resulted in greater bioadhesion, resulting from an increased number of sites available for hydrogen bonds [64]. All this prior work, including the current data, gives promise that pectin could result in suitable bioadhesion to hold NPs in place once sprayed into a resection cavity.

4.4. Gel formation at calcium concentrations found within the brain

One concern was whether pectin would gel within the calcium concentration range (1.5–2 mM) of the brain extracellular space. To address this, the pectin solution was sprayed onto TLC plates soaked with 1.5 mM of calcium chloride. The gelling capability was measured in terms of pectin drip length when sprayed onto a surface at 45°, which was compared to a control solution of water sprayed onto the same surface. The drip length was determined from the bottom of the impact area to the bottom of the drip, as shown by the red arrows on the inset image in Fig. 1F. This methodology was adapted from a study by Castile et al. [39], which used the inclined TLC plate method to analyse dripping of pectin-based nasal spray technology. They found a significant reduction in drip length when 10 mg/mL LM pectin was used, relative to the non-gelling (PBS) control when spraying onto a TLC plate soaked in simulated nasal electrolyte solution ($CaCl_2H_4O_2$ concentration of 4 mM).

Similarly, our data shows that there was a significant decrease in drip length when a calcium-soaked TLC plate was used instead of a water-soaked TLC plate, demonstrating gelling of the 200 μM pectin solution.

4.5. In vivo retention and biocompatibility of pectin in a brain resection site

Following promising *in vitro* results showing a lack of toxicity to U87 cells, some biocompatibility with primary human astrocytes and signs of degradation in aCSF, *in vivo* retention and toxicological analysis of the pectin gel was carried out. To our knowledge pectin has not previously been implanted into the brain, despite many other *in vivo* assessments such as the subcutaneous implantation injection of >2.5% (w/v) pectin gels in mice, showing no toxicity over 7 days [56]. Therefore, to determine whether the pectin gel was fit-for-purpose for the intended DDS, it was orthotopically injected into the brains of mice and left for up to two weeks.

Pectin was labelled so that approximately 5% of carboxylic acid groups within the pectin backbone would contain a Cy5 label. Pectin requires the carboxylic acid groups to gel in the presence of calcium, therefore labelling too many of these groups would hinder the gelling capability of pectin. This Cy5-pectin powder was combined with non-labelled pectin powder at 3% (w/w) which was previously found to generate a strong signal using an *in vivo* Imaging System (IVIS) (data not shown). A 200 µM pectin gel was chosen for *in vivo* analysis as it was generally biocompatible in the *in vitro* analyses. Furthermore, a higher concentration of pectin generates a more bioadhesive gel due to the ability to form greater hydrogen bonds to brain tissue [64], thus fulfilling the purpose of the hydrogel (to remain in the tissue it is sprayed into).

Following injection, animals were immediately imaged using the IVIS to reveal the location and intensity of the pectin signal and to provide a baseline signal. This time point showed maximum baseline fluorescence, which could then be tracked over time to show any potential retention or loss of pectin in the brain, directly corresponding to Cy5 degradation/elimination. Fig. 2A shows an image from the IVIS of animals at 24 h post-pectin injection (with all IVIS images shown in Fig. Supplementary Fig. S3). The data in 2B shows that at 24 h, the fluorescence observed in *ex vivo* brains was significantly higher than the control baseline signal (sham surgery only), showing good initial retention of pectin at the injection site. At day 14, the fluorescence had decreased to baseline levels, showing no significant difference between the control and the Cy5-pectin injected animals, providing yet further evidence that pectin degrades within the brain.

Over the time course of this experiment, there was no neurotoxicity evident in any of the animals; specifically, no weight loss nor behavioural changes were observed, indicating that pectin had not likely caused any adverse effects due to exposure within the brain. However, to corroborate this evidence, haematoxylin and eosin (H&E) stains were carried out on sections of post-sacrificial mouse brains to determine if there was any evidence of a local inflammatory response. As shown in Fig. 2C, there appears to be no change in local cell morphology or sign of an influx of cells indicative of inflammation, compared to the control section, at 24 h post-surgery.

4.6. NCPP structure

Following the successful determination of a hydrogel fit-for-purpose within the brain, we then developed NPs, which would later be held within this pectin gel. NPs were developed using a novel method of generating drug nanocrystals before coating in a polymeric layer to provide a steric barrier. To prove successful coating of the drug
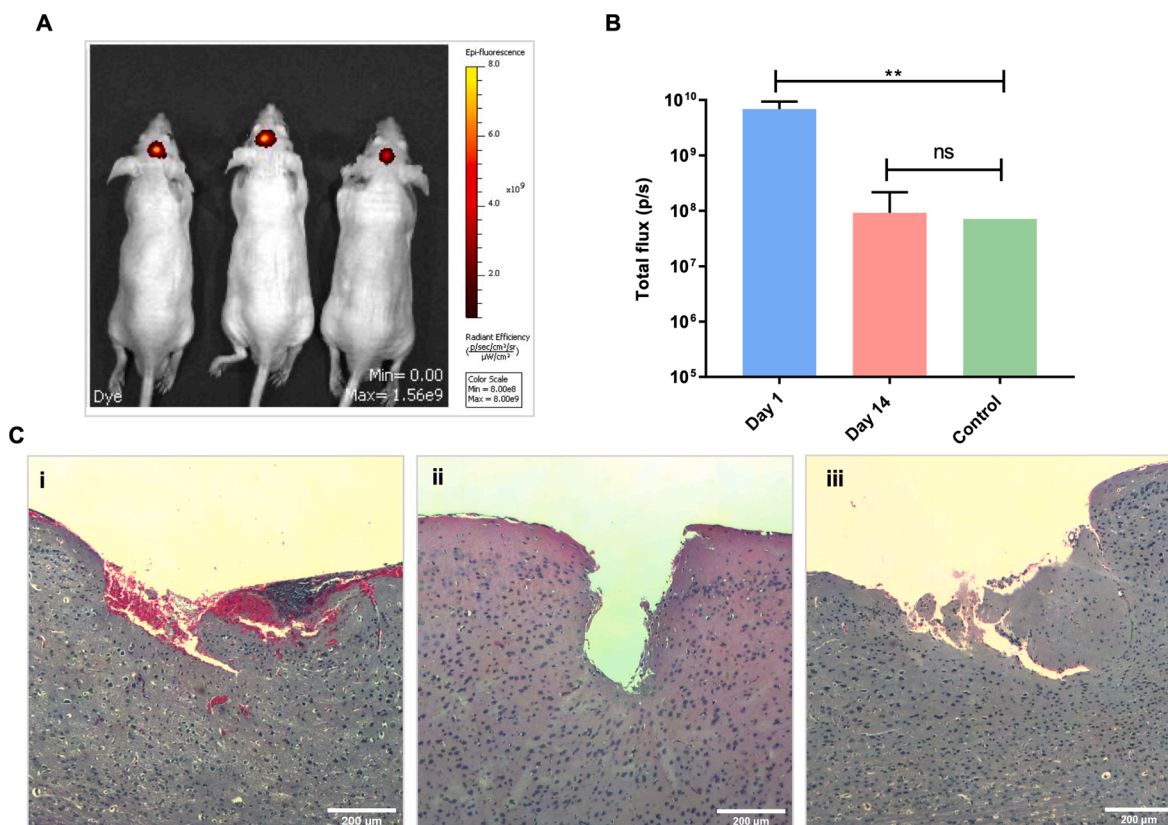
Fig. 2. In vivo retention and biocompatibility of pectin hydrogel. (A) IVIS image of nude mice following a stereotactic injection of Cy5-labelled pectin into the brain. Image taken at 24 h following surgery. (B) *Ex vivo* Cy5 fluorescence detected in the brains by the IVIS. Retention was shown at 24 h with a significant reduction in fluorescence observed at 14 days following surgery when using a one-way ANOVA with Dunnett's post-hoc test when compared to the control animal. ** = P < 0.01. (C) Haematoxylin and Eosin stained brain sections from (i) sham surgery control animal and (ii, iii) pectin injected animals, sacrificed at 24 h post-surgery, showing no difference in cellular morphology relative to sham surgery controls.

nanocrystals, TEM and DLS were used. Prior to adding a polymer coating, the drug nanocrystal had a z-average between 100 and 300 nm with variable and multiple peaks observed within samples, and with large PDI values (>0.3). As shown in Fig. 3A, etoposide nanocrystals at 0.25 mg/mL, had an average size of 112 nm and a PDI of 0.345, with large error bars showing differences between individual samples; however, when coated with 0.25 mg/mL polymer, this reduced to 68 nm and a PDI of 0.232. This was also observed for olaparib nanocrystals, which showed clear aggregates that were not present when there was polymer in the formulation (Fig. 3B). This suggests that there could be some solvent-nanocrystal and drug-polymer interactions occurring, which may have caused the drug to disaggregate, allowing the formation of a smaller, coated NP [19].

From TEM images, nanocrystals, when compared to NCPPs, reveal visible differences in structure, providing evidence for NCPPs (rather than two distinct populations). Fig. 3C shows both etoposide and olaparib NCPPs were visibly different from the larger and heterogeneously sized drug nanocrystals. The NCPPs had a double shell structure, with

the core exhibiting a lower contrast than the shell, thus giving evidence for true polymer-coated drug NPs (more representative TEM images can be seen in Fig. Supplementary Fig. S4). Further comparisons of zeta potential (ZP) data from drug nanocrystals and polymer-only NPs, compared to NCPPs corroborate TEM and DLS results. The ZP curves reveal multiple peaks for non-coated drug nanocrystals, which shifts to the same value as the polymer control when the drug was coated (Fig. 3D-E). A recent publication by Styliari et al., suggested very similar results when coating indomethacin with a PEG-polycaprolactone diblock copolymer. Although the methodology to generate the NCPPs was different (flow nanoprecipitation), the study also found differences in DLS and TEM data, before and after coating with amphiphilic polymer. The report suggested that the addition of the solvent/polymer may have broken up larger drug aggregates, allowing the coating of smaller individual drug NPs [19], which supports our findings.
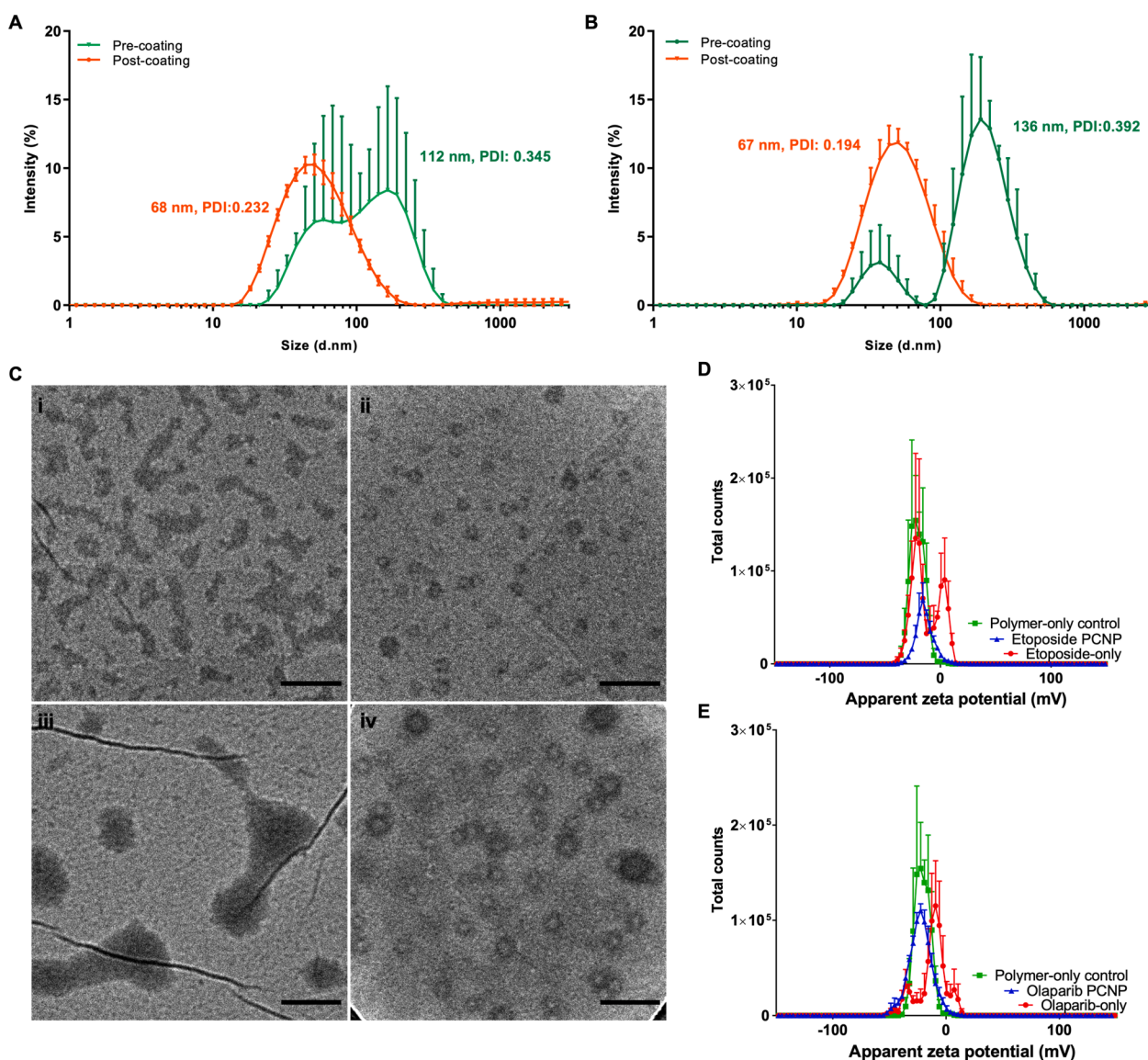
Fig. 3. Size distribution profiles and visualisation of NCPPs. (A) DLS curves of 0.25 mg/mL etoposide pre- (112 ± 16 nm, PDI: 0.345 ± 0.196) and post-coating with 0.25 mg/mL mPEG$_{5000}$-PLA$_{100}$ (68 ± 2 nm, PDI: 0.232 ± 0.044), and (B) 0.25 mg/mL olaparib pre- (136 ± 19 nm, PDI: 0.393 ± 0.221) and post-coating with 0.25 mg/mL mPEG$_{5000}$-PLA$_{100}$ (67 ± 1 nm, PDI: 0.194 ± 0.017). Results are shown as mean ± SD, $n = 3$. (C) TEM images taken at 20,000× magnification of: i) 0.25 mg/mL etoposide in water; ii) 0.25 mg/mL etoposide NCPPs; iii) 0.25 mg/mL olaparib in water; iv) 0.25 mg/mL olaparib NCPPs. Scale bar = 100 nm. (D) Zeta potential of 0.25 mg/mL etoposide NCPPs and (E) 0.25 mg/mL olaparib NCPPs versus polymer-only and drug-only controls. Results are shown as mean ± SD, $n = 3$.

4.7. NCPP stability and drug release

The stability of NCPPs was then studied in different aqueous media at 37 °C for up to 24 h. Fig. 4A shows the etoposide NCPPs in PBS, DMEM and aCSF, confirming high stability at 24 h. The PDI of all samples did not significantly increase over the time course, representing a mono-disperse system. Fig. 4B shows the same results for olaparib NCPPs, whereby there was no significant increase in size nor PDI up to 24 hrs. Previous work showed stability of these PLA-PEG based NPs when incubated with bovine serum albumin, displaying their ability to resist any protein-induced aggregation; the study also demonstrated NP stability to increasing NaCl concentrations [45] and although these were polymer-only NPs, this indicates inherent high stability of these NPs.

Initial drug loading of the NCPPs was 32% and 33% for etoposide and olaparib, respectively. These NCPPs were then subjected to increased concentrating via N_2 gas evaporating off the aqueous phase. Final HPLC of these NCPPs showed an absolute drug concentration of 0.30 ± 0.01 mg/mL and 0.24 ± 0.05 mg/mL (mean $\pm$ SD, $n = 3$), for etoposide and olaparib NCPPs, respectively. For etoposide, this level of drug loading exceeds that shown in the majority of previous studies; for PEG-PLA based NPs, a drug loading of 9.6% has been shown [65]; however a study by Saadati et al. [66] reported drug loading which was dependent on the method of NP preparation where PLGA-PEG NPs generated by nanoprecipitation had an etoposide drug loading of 7%

and those generated by solvent evaporation had a drug loading of 12%. This distinct methodology could be one factor which has led to the high drug loading of these polymer NPs. This is also corroborated by Styliari et al., having demonstrated a drug loading of 78% for indomethacin using a similar coating strategy [19]. For olaparib, there are few poly-meric NPs reported in the literature. Wu et al. [67] manufactured PEG-poly e-caprolectone NPs with an olaparib drug loading as high as 10%; however, to the best of our knowledge, no PLA-PEG based olaparib NPs have been reported.

Drug release was analysed over 120 h with the results in Fig. 4C and D displaying that release from the concentrated NCPPs was rapid, with a burst release of 5% for olaparib in the first 30 min followed by 85% after 24 h. Likewise, for the etoposide sample, there was a burst of 9% in the first 30 min followed by 83% after 24 h. In both cases, 100% drug release was released after 48 h. However, when the NCPPs were incubated with pectin, 20% of olaparib seemed to be trapped within the hydrogel. This was likely a result of hydrophobic interactions between the esterified regions of the pectin gel and olaparib molecules [68]. Rapid release of drug from these NPs means that the drug may potentially be released immediately post-surgery, at a time when there is the lowest residual tumour burden within the brain. Following maximal surgical resection, there are few cells left within the healthy brain tissue and therefore targeting these cells before rapid proliferation and bulk tumour recur-rence is likely to generate higher efficacy of the chemotherapies.
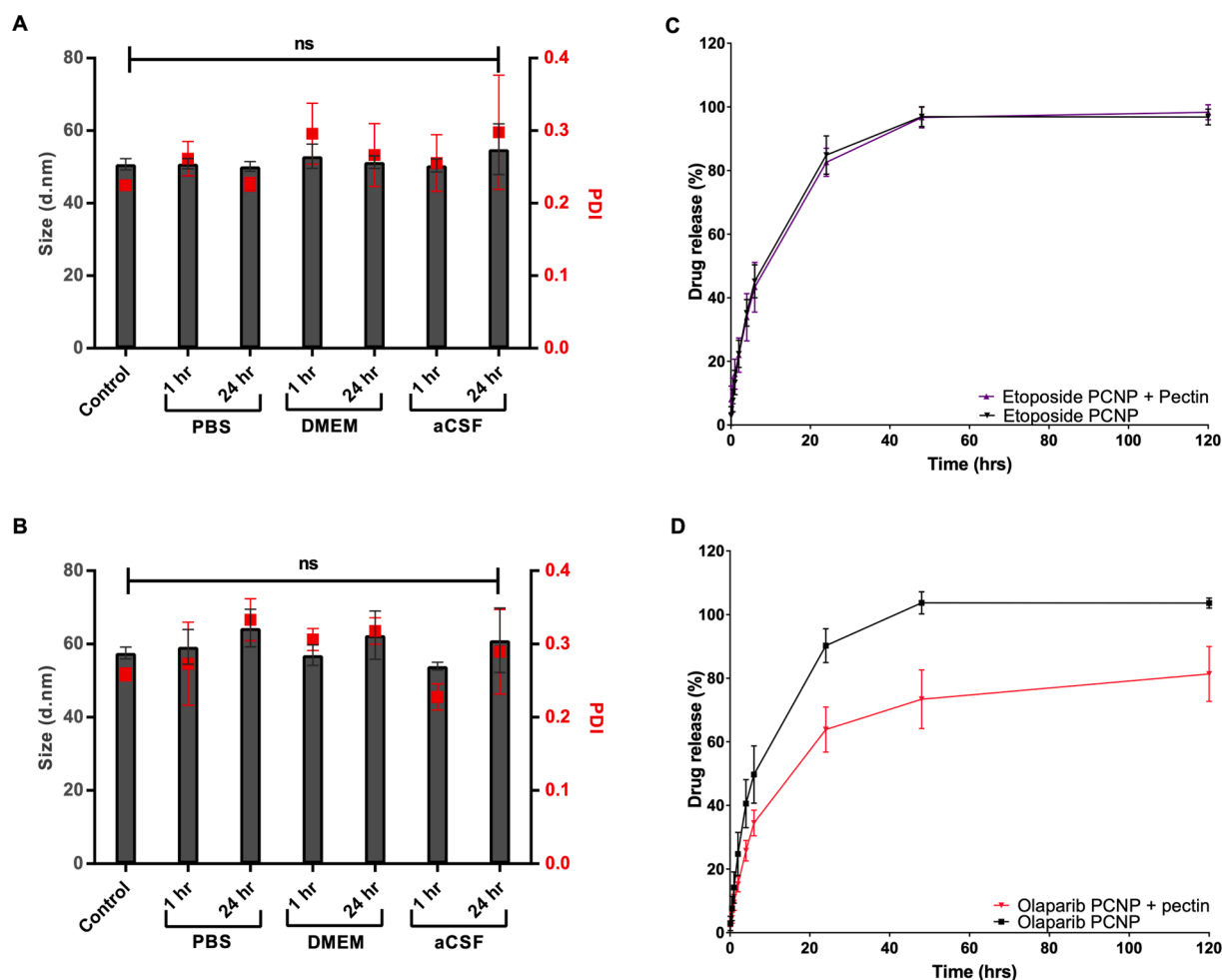
Fig. 4. In vitro characterisation and release profiles for drug-loaded polymeric nanoparticles. Size and PDI of (A) etoposide and (B) olaparib NCPPs following incubation with PBS, DMEM and aCSF at 1 and 24 h. No dilution of NCPPs was necessary for the DLS measurements. Results displayed as mean $\pm$ SEM, no sig-nificance was found in a one-way ANOVA with a Dunnett's post-hoc test, when compared to the control, n = 3. (C) Drug release into 10% w/v HPßCD in water from etoposide NCPPs and (D) olaparib NCPPs $\pm$ 200 μM pectin gel over 120 h at 37 °C, showing 9% and 5% release in the first 30 min followed by 85% and 83% after 24 h for etoposide and olaparib, respectively. Results are displayed as mean $\pm$ SD, $n = 4$.

4.8. Biocompatibility of NPs with astrocytes

Biocompatibility of the DDS is paramount for successful use within the brain; therefore, biocompatibility of polymeric NPs with 'healthy' matter within the brain was studied by incubating 0.0625 to 1 mg/mL NPs (no drug) with human astrocytes. Fig. Supplementary Fig. S5 shows that there was no significant reduction in astrocyte viability over 72 h at any concentration. These results were anticipated due to the plethora of literature showing good biocompatibility of PLA-PEG based NPs [25–27].

Characterisation of these NCPPs established that they were fit-for-purpose for the DDS under development, henceforth they, alongside the pectin hydrogel, were trialled with the spray device.
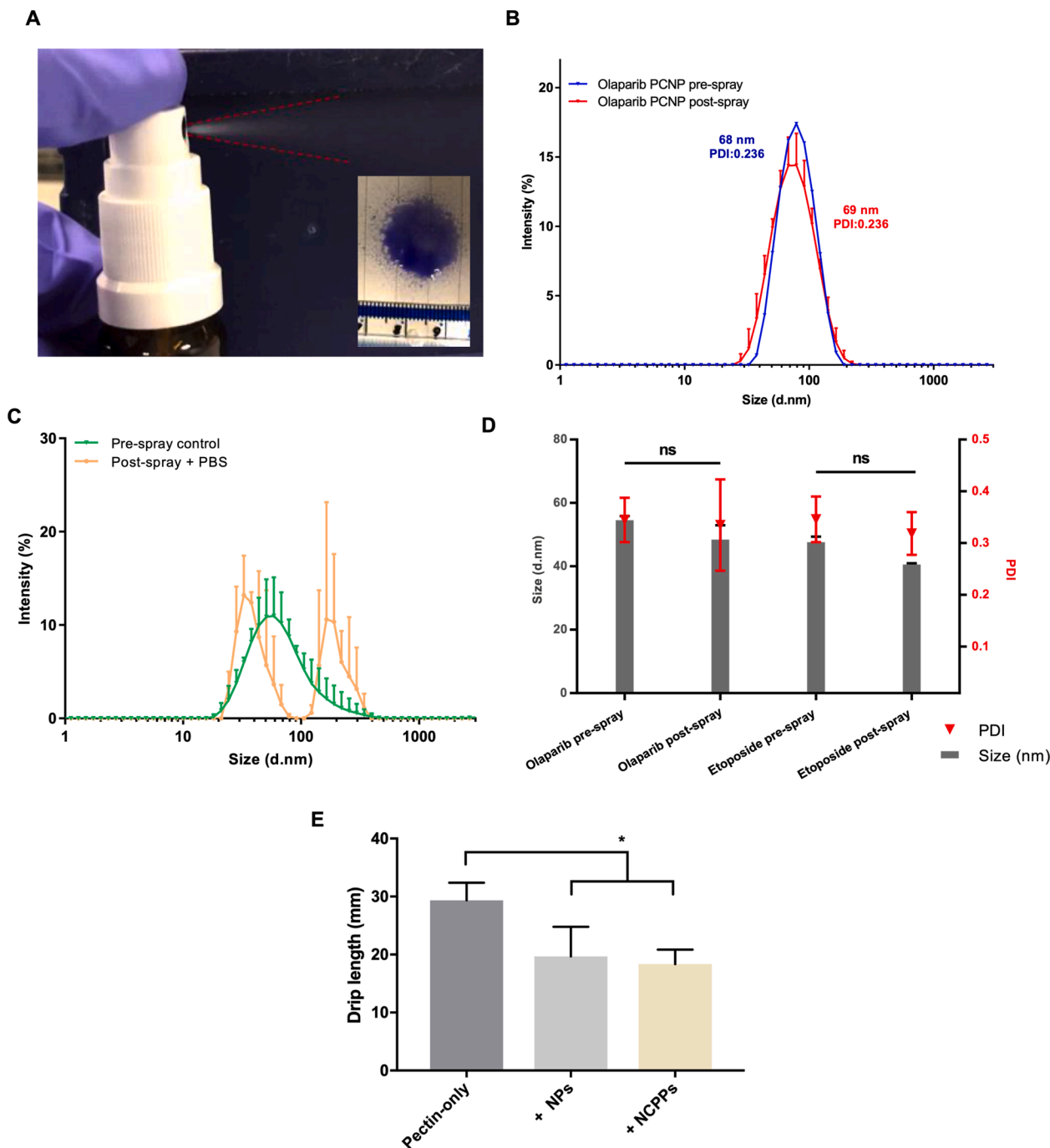
Fig. 5. In vitro spray characterisation of pectin and drug-loaded nanoparticles. (A) Image showing the successful spray mist, with the inset image showing the spray pattern. (B) DLS curves of 0.25 mg/mL olaparib NCPPs in water pre- (68 ± 3 nm, PDI: 0.236 ± 0.089) and post-spray (69 ± 2 nm, PDI: 0.236 ± 0.102), with results displayed as mean $\pm$ SD, $n = 4$. (C) DLS curves of 0.25 mg/mL olaparib NCPPs in 0.01 M PBS pre- (109 ± 4 nm, PDI: 0.256 ± 0.011) and post-spray (236 ± 201 nm, PDI: 0.400 ± 0.097), with results shown as mean $\pm$ SD, $n = 4$. (D) Bar chart showing size and PDI values of 0.25 mg/mL etoposide and olaparib NCPPs in 0.01 M PBS and 0.5% w/v PF127, pre- and post-spray. Results are displayed as mean $\pm$ SD, $n = 3$. No significance between pre- and post-spray was found when using a two-tailed t test. (E) Drip lengths of a 200 μM pectin solution $\pm$ polymer-only NPs pr NCPPs sprayed onto TLC plates soaked in 1.5 mM CaCl$_2$. TLC plates were fixed at a 45° angle and the drip length was measured. Results are displayed as mean $\pm$ SEM, $n = 6$, with a significant reduction in drip length determined using a one-way ANOVA with Dunnett's post-hoc test. * = P < 0.05.

4.9. Spraying of the formulation

Successful spraying of the viscous hydrogel solution is shown in Fig. 5A, whereby a 200 μM pectin gel with a blue dye shows the spray pattern when 50 μL was sprayed. Fig. Supplementary Fig. S6 shows the volumes per spray from the device, demonstrating consistent and correct volumes sprayed. This device was then trialled with the NPs in solution. As shown in Fig. 5B, when a solution of olaparib NCPPs in milliQ water aqueous phase plus 0.5% HPβCD to aid stability, was sprayed, there was no change in NP size nor appearance of a second peak indicative of aggregation. This data was the same for etoposide NCPPs (Fig. Supplementary Fig. S7). However, when introducing PBS into this aqueous phase (Fig. 5C), the results showed that the NPs aggregated, despite the HPβCD sugar presence in the formulation.

The steric barrier of the polymer is clearly sufficient at preventing NCPP aggregation, as previously shown in the PBS samples in Fig. 4A and B. However, when the NCPPs are subjected to shear stress when forced through the spray nozzle, the polymeric layer may not be able to overcome the reduced dispersion of NPs within the small droplet volume of the spray mist, nor the attractive Van der Waals forces and the reduced electric double-layer repulsion when PBS is present [69–72], thus likely leading to aggregation. A paper by Hendriks et al., showed how cell viability decreased when spray pressure increased. The reduced viability was proposed to be as a result of smaller spray droplets being formed due to this increase in pressure. These smaller drops impacted with the surface at higher velocities, which led to increased cell deformation and thus cell death [73]. Although cells are very different to our application, the concept is the same for NPs. With increasing pressure (and shear stress), the spray droplets formed will be smaller, causing a reduction in the dispersion of the NPs within this droplet. This, alongside the impact speed from increased pressure, is likely to deform and aggregate the NPs. Furthermore, a study by Jeong et al. [74] commented on adhesive mussel-protein based NPs for locoregional cancer therapy, and their stability to spray, which the authors attributed to the low PBS concentration and ethanol content (30:70 v/v). The study suggests high dispersion of NPs is key to successful spraying, as low dispersion of NPs allows aggregation when the NPs pass through the nozzle. In this instance, the low PBS concentration allowed electrostatic repulsion of the NPs, and the low surface tension of ethanol removed chances of aggregation. However, such a high ethanol concentration would likely prove toxic to the human brain; high concentrations of ethanol in the brain make it vulnerable to ethanol-induced reactive oxygen species (ROS) due to its high content of peroxidable fatty acids [75,76] and therefore it was not suitable for use in this application.

It could not be determined whether the viscous pectin solution enhanced survival of the NCPPs as pectin sequesters the NCPPs, which rendered them being undetectable on the DLS. The solution state pectin was also unstable when imaged using TEM, meaning conclusive evidence could not be gathered for NCPP survival. Therefore, we explored the addition of a surfactant in the aqueous phase.

PF127 was then added to the formulation instead of HPβCD, to assess if this provided stabilising properties when PBS was present in the formulation. PF127 is FDA approved and has been widely used *in vivo* due to its relatively non-toxic and biodegradable properties [77]. Previous studies have reported PF127 gel use within the brain up to 18% (w/v) with no associated side effects [78,79]. Other formulations have used PF127 between 0.13 and 13% (w/v) to stabilise silver NPs [80] and shown that Pluronics (F127 and F108) provide greater steric stability to PLGA-NPs. The Pluronics made the system less sensitive to increases in ionic strength, proven by the increased critical aggregation concentration [81]; therefore PF127 was tested within our system. A 5% PF127 solution in 0.1 M PBS (w/v) was added to the NCPP formulation, generating a final concentration of 0.5% PF127 and 0.01 M PBS. The results are shown in Fig. 5D, showing no significant change in NP size nor PDI following spraying.

We have so far demonstrated that pectin gelled in the presence of

calcium concentrations equivalent to those found within the brain. However, we also wanted to assess any changes brought about by NPs or NCPPs within the pectin formulation. Therefore, to assess the effects of polymer-only NPs and NCPPs on the ability of pectin to gel, pectin solution with and without NPs was sprayed onto an inclined TLC plate soaked in 1.5 mM CaCl₂ (as before). As shown in Fig. 5E, there was a significant (P < 0.05) reduction in drip length of 200 μM pectin when in the presence of NPs or NCPPs. There was no difference between the two NP formulations (with or without drug), which was anticipated due to the drug residing in the centre of the NCPP, thus not interacting with the pectin medium. A change in viscosity between the pectin control and pectin with NPs was anticipated as it has previously been demonstrated that a hydrogel in the presence of NPs exhibits different physio-chemical properties as a result of non-covalent interactions [82]. It is likely that the non-covalent interactions between the NPs and hydrogel have increased the viscosity of the formulation, thus reducing the measured drip length.

4.10. Application of the DDS to a large mammalian brain

Following the completion of hydrogel and NCPPs characterisation with the spray device, the DDS was trialled in an *ex vivo* porcine brain, representative of a large mammalian brain to show if the DDS was fit-for-purpose. In this experiment, Cy5-labelled polymer-only NPs were trialled in the brain for confocal microscopy analysis. No drug was present within the NPs in order to simplify the detection of the NPs within brain tissue. Despite the lack of drug in the NP, this work still presents the benefit of spraying the optimal formulation into a resection cavity.

Pectin (200 μM) with Cy5 labelled NPs at equal size to the NCPPs (70 ± 15 nm [mean ± SD, *n* = 15]) was sprayed into the linings of a surgical pseudo-resection cavity and sequential biopsies taken from below this cavity to determine successful delivery of the system and assess depth of penetration. Confocal microscopy shown in Fig. 6 displayed NP presence in the biopsy tissue up to 1.5 cm deep. As the study by Nance et al. suggests, this result was anticipated due to the size (70 nm) and PEGylation (mPEG₅₀₀₀) of the NPs, conferring decreased interactions with brain tissue [11] and confirming our DDS design. From the confocal images, it seems that there is a greater accumulation of fluorescence observed in biopsy 3. It would be anticipated that the greatest fluorescence seen would be in biopsy 1 due to the site of application however, this depends on the area and the orientation of the biopsy which has been sectioned. For biopsy 3, there could have been a reservoir of NPs which had built up due to a white matter tract leading to this area, and we could also have sectioned a tissue region which contained more NPs, relative to other regions. Nevertheless, this technique was a qualitative means to determine NP penetration in a large mammalian brain, showing high success of NP translocation post-spray into a surgical cavity.

5. Conclusion

A DDS has been developed which uses a spray device to successfully deliver a bioadhesive hydrogel and high etoposide and olaparib loaded polymeric NPs to a surgical resection site. Pectin solution can be sprayed successfully, and it has proven to be bioadhesive and which gels in the presence of calcium concentrations found locally within the brain. To our knowledge, this is the first report to show biocompatibility within the brain *in vivo*, with no neurotoxicity in animals observed over two weeks. We have developed two novel polymer-coated nanoparticle formulations at ~70 nm, with drug concentrations of 0.30 and 0.24 mg/mL for etoposide and olaparib respectively. These NCPPs are stable in different media such as aCSF, DMEM and PBS, can survive the shear stress of a spray device and release therapeutic cargo rapidly over 48 h. We have demonstrated clinical utility of this DDS via NP delivery within a surgical pseudo-resection cavity in large mammalian brain, revealing
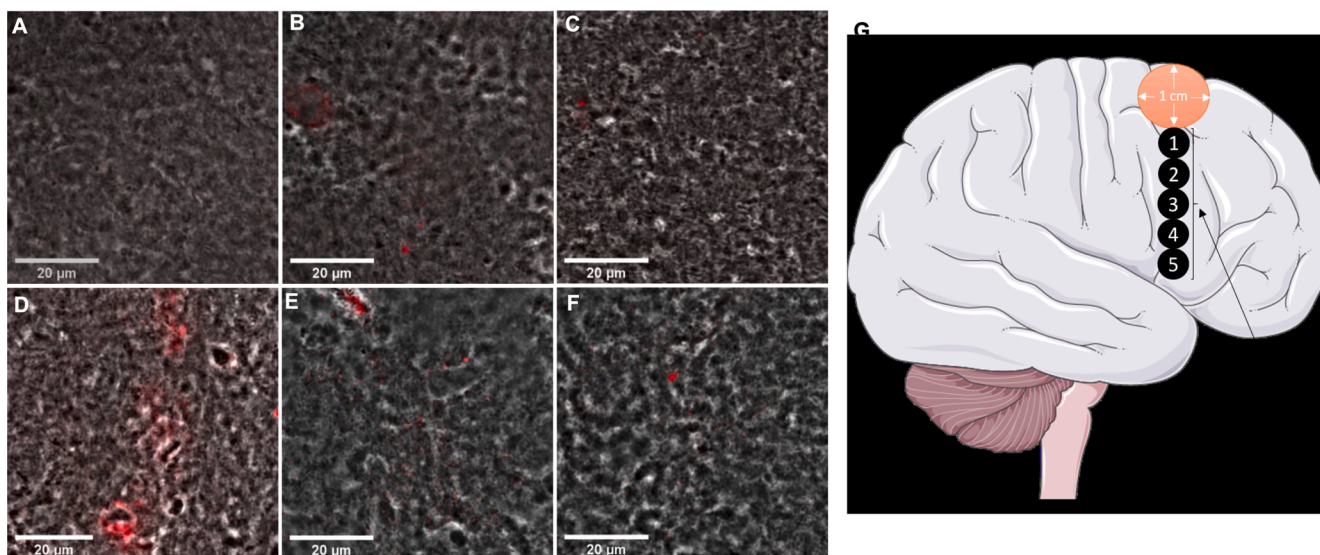
Fig. 6. Visualisation of sprayed fluorescent-labelled polymeric nanoparticles using a large mammalian brain *ex vivo*. 0.25 mg/mL Cy5-labelled mPEG$_{5000}$-PLA$_{100}$ NPs in 200 µM pectin plus 0.5% PF127 and 0.01 M PBS solution sprayed into a pseudo-resection margin of an *ex vivo* cadaver porcine brain. Confocal images of cryosectioned brain show (A) control section, (B-F) fluorescent NPs within brain tissue in sequential biopsies taken from the cavity downwards, as depicted by numbers 1–5 in the schematic shown in (G). Schematic (not to scale) illustrating sequential biopsies, where actual distance is approximately 1.5 cm deep into the tissue.

the presence of NPs in the surrounding tissue up to 1.5 cm away from the cavity. Our data collectively demonstrates the pre-clinical development of a novel DDS based on a sprayable hydrogel containing therapeutic NCPPs, which is amenable for translation to orthotopic brain tumour surgical resection models to assess efficacy upon localised delivery.

Funding

Declaration of Competing Interest

The authors have no competing interests to declare.

Appendix A. Supplementary material

Supplementary data to this article can be found online at https://doi.org/10.1016/j.ejpb.2020.10.005.

References

[1] M. Koshy, et al., Improved survival time trends for glioblastoma using the SEER 17 population-based registries, J. Neurooncol. 107 (2012) 207–212.
[2] R. Stupp, et al., Effects of radiotherapy with concomitant and adjuvant temozolomide versus radiotherapy alone on survival in glioblastoma in a randomised phase III study: 5-year analysis of the EORTC-NCIC trial, Lancet Oncol. 10 (2009) 459–466.
[3] R. Stupp, et al., Radiotherapy plus concomitant and adjuvant temozolomide for glioblastoma, N. Engl. J. Med. 352 (2005) 987–996.
[4] M.E. Hegi, et al., MGMT gene silencing and benefit from temozolomide in glioblastoma, N. Engl. J. Med. 352 (2005) 997–1003.
[5] S. Deorah, C.F. Lynch, Z.A. Sibenaller, T.C. Ryken, Trends in brain cancer incidence and survival in the United States: Surveillance, Epidemiology, and End Results Program, 1973 to 2001, Neurosurg. Focus 20 (2006) E1.
[6] D.R. Johnson, B.P. O'Neill, Glioblastoma survival in the United States before and during the temozolomide era, J. Neurooncol. 107 (2012) 359–364.
[7] T.H. Ung, H. Malone, P. Canoll, J.N. Bruce, Convection-enhanced delivery for glioblastoma: targeted delivery of antitumor therapeutics, CNS Oncol. 4 (2015) 225–234.
[8] C. Bastianich, P. Danhier, V. Preat, F. Danhier, Anticancer drug-loaded hydrogels as drug delivery systems for the local treatment of glioblastoma, J. Control. Release 243 (2016) 29–42.

[9] N.B. Roberts, et al., Repurposing platinum-based chemotherapies for multi-modal treatment of glioblastoma, Oncoimmunology 5 (2016) e1208876.
[10] E. Alphandéry, Nano-therapies for glioblastoma treatment, Cancers (Basel) 12 (2020) 242.
[11] E.A. Nance, et al., A dense poly(ethylene glycol) coating improves penetration of large polymeric nanoparticles within brain tissue, Sci. Transl. Med. 4 (2012) 149ra119.
[12] E. Nance, et al., Brain-penetrating nanoparticles improve paclitaxel efficacy in malignant glioma following local administration, ACS Nano 8 (2014) 10655–10664.
[13] S.J. Smith, et al., Overall survival in malignant glioma is significantly prolonged by neurosurgical delivery of etoposide and temozolomide from a thermo-responsive biodegradable paste, Clin. Cancer Res. 25 (2019) 5094–5106.
[14] S. Smith, et al., Neurosurgical delivery of the poly ADP ribose polymerase-1 inhibitor olaparib from a thermo-responsive biodegradable paste potentiates radiotherapy and prolongs survival, Neuro. Oncol. 21 (2019) iv2–iv2.
[15] Y.C. Kuo, Y.C. Chen, Targeting delivery of etoposide to inhibit the growth of human glioblastoma multiforme using lactoferrin- and folic acid-grafted poly (lactide-co-glycolide) nanoparticles, Int. J. Pharm. 479 (2015) 138–149.
[16] A.J. Chalmers, Science in focus: combining radiotherapy with inhibitors of the DNA damage response, Clin. Oncol. 28 (2016) 279–282.
[17] C.V.M. Verhagen, et al., Extent of radiosensitization by the PARP inhibitor olaparib depends on its dose, the radiation dose and the integrity of the homologous recombination pathway of tumor cells, Radiother. Oncol. 116 (2015) 358–365.
[18] B. Fulton, et al., PARADIGM-2: Two parallel phase I studies of olaparib and radiotherapy or olaparib and radiotherapy plus temozolomide in patients with newly diagnosed glioblastoma, with treatment stratified by MGMT status, Clin. Transl. Radiat. Oncol. 8 (2018) 12–16.
[19] I.D. Styliari, et al., Nanoformulation-by-design: an experimental and molecular dynamics study for polymer coated drug nanoparticles, RSC Adv. 10 (2020) 19521–19533.
[20] N.T.K. Thanh, N. Maclean, S. Mahiddine, Mechanisms of nucleation and growth of nanoparticles in solution, Chem. Rev. 114 (2014) 7610–7630.
[21] A. Abushrida, et al., A simple and efficient method for polymer coating of iron oxide nanoparticles, J. Drug Deliv. Sci. Technol. 55 (2020) 101460.
[22] T. Pellegrino, et al., Hydrophobic nanocrystals coated with an amphiphilic polymer shell: A general route to water soluble nanocrystals, Nano Lett. 4 (2004) 703–707.
[23] G. Palui, F. Aldeek, W. Wang, H. Mattoussi, Strategies for interfacing inorganic nanocrystals with biological systems based on polymer-coating, Chem. Soc. Rev. 44 (2015) 193–227.
[24] T.Y. Kim, et al., Phase I and pharmacokinetic study of Genexol-PM, a Cremophor-free, polymeric micelle-formulated paclitaxel, in patients with advanced malignancies, Clin. Cancer Res. 10 (2004) 3708–3716.
[25] K. Hu, et al., Lactoferrin-conjugated PEG-PLA nanoparticles with improved brain delivery: In vitro and in vivo evaluations, J. Control. Release 134 (2009) 55–61.
[26] A. Vila, H. Gill, O. McCallion, M.J. Alonso, Transport of PLA-PEG particles across the nasal mucosa: Effect of particle size and PEG coating density, J. Control. Release 98 (2004) 231–244.
[27] V. Shalgunov, et al., Comprehensive study of the drug delivery properties of poly (L-lactide)-poly(ethylene glycol) nanoparticles in rats and tumor-bearing mice, J. Control. Release 261 (2017) 31–42.

[28] J. Li, D.J. Mooney, Designing hydrogels for controlled drug delivery, Nat. Rev. Mater. 1 (2016).

[29] H. Brem, et al., Interstitial chemotherapy with drug polymer implants for the treatment of recurrent gliomas, J. Neurosurg. 74 (1991) 441–446.

[30] K.O. Lillehei, et al., Rationale and design of the 500-patient, 3-year, and prospective Vigilant ObservatIon of gliadel wafer implant registry, CNS Oncol. 7 (2018) CNS08.

[31] S.J. Smith, et al., Surgical delivery of drug releasing poly(lactic-co-glycolic acid)/poly(ethylene glycol) paste with in vivo effects against glioblastoma, Ann. R. Coll. Surg. Engl. 96 (2014) 495–501.

[32] Y. Zhang, et al., A Bioadhesive nanoparticle-hydrogel hybrid system for localized antimicrobial drug delivery, ACS Appl. Mater. Interfaces 8 (2016) 18367–18374.

[33] Q. Feng, et al., Mechanically resilient, injectable, and bioadhesive supramolecular gelatin hydrogels crosslinked by weak host-guest interactions assist cell infiltration and in situ tissue regeneration, Biomaterials 101 (2016) 217–228.

[34] E.F. Kong, et al., Development and in vivo evaluation of a novel histatin-5 bioadhesive hydrogel formulation against oral candidiasis, Antimicrob. Agents Chemother. 60 (2016) 881–889.

[35] D. Lootens, et al., Influence of pH, Ca concentration, temperature and amidation on the gelation of low methoxyl pectin, Food Hydrocoll. 17 (2003) 237–244.

[36] B.R. Thakur, R.K. Singh, A.K. Handa, M.A. Rao, Chemistry and uses of pectin-A review, Crit. Rev. Food Sci. Nutr. 37 (1997) 47–73.

[37] A. Sundar Raj, S. Rubila, R. Jayabalan, T. Ranganathan, A Review on pectin: chemistry due to general properties of pectin and its pharmaceutical uses, Open Access Sci. Reports 1 (2012).

[38] D.M. Egelman, P. Read Montague, Calcium dynamics in the extracellular space of mammalian neural tissue, Biophys. J. 76 (1999) 1856–1867.

[39] J. Castile, et al., Development of in vitro models to demonstrate the ability of PecSys®, an in situ nasal gelling technology, to reduce nasal run-off and drip, Drug Dev. Ind. Pharm. 39 (2013) 816–824.

[40] P.H. Maurer, B. Berardinelli, Immunologic Studies with Hydroxyethyl Starch (HES) A Proposed Plasma Expander, Transfusion 8 (1968) 265–268.

[41] D.B. Kendrick, Blood program in World War II : supplemented by experiences in the Korean War, Washington, D.C., 1989.

[42] Y. Wu, S. Joseph, N.R. Aluru, Effect of cross-linking on the diffusion of water, ions, and small molecules in hydrogels, J. Phys. Chem. B 113 (2009) 3512–3520.

[43] J. Trudel, S.P. Massia, Assessment of the cytotoxicity of photocrosslinked dextran and hyaluronan-based hydrogels to vascular smooth muscle cells, Biomaterials 23 (2002) 3299–3307.

[44] M.C. Tate, D.A. Shear, S.W. Hoffman, D.G. Stein, M.C. LaPlaca, Biocompatibility of methylcellulose-based constructs designed for intracerebral gelation following experimental traumatic brain injury, Biomaterials 22 (2001) 1113–1123.

[45] H. Phan, et al., Role of self-assembly conditions and amphiphilic balance on nanoparticle formation of PEG-PDLLA copolymers in aqueous environments, J. Polym. Sci. Part A Polym. Chem. 57 (2019) 1801–1810.

[46] F. Sodano, et al., Enhancing doxorubicin anticancer activity with a novel polymeric platform photoreleasing nitric oxide, Biomater. Sci. 8 (2020) 1329–1344.

[47] A. Zgair, et al., Development of a simple and sensitive HPLC-UV method for the simultaneous determination of cannabidiol and δ9-tetrahydrocannabinol in rat plasma, J. Pharm. Biomed. Anal. 114 (2015) 145–151.

[48] P. Daumar, et al., Development and validation of a high-performance liquid chromatography method for the quantitation of intracellular PARP inhibitor Olaparib in cancer cells, J. Pharm. Biomed. Anal. 152 (2018) 74–80.

[49] K.J. Bronsema, R. Bischoff, N.C. Van de Merbel, Internal standards in the quantitative determination of protein biopharmaceuticals using liquid chromatography coupled to mass spectrometry, J. Chromatogr. B 893–894 (2012) 1.

[50] A.H. Algan, M. Gumustas, A. Karatas, S.A. Ozkan, A selective and sensitive stability-Indicating HPLC method for the validated assay of etoposide from commercial dosage form and polymeric tubular nanocarriers, J. Pharm. Biomed. Anal. 124 (2016) 382–389.

[51] A. Beig, et al., Head-to-head comparison of different solubility-enabling formulations of etoposide and their consequent solubility-permeability interplay, J. Pharm. Sci. 104 (2015) 2941–2947.

[52] L. Morosi, et al., Quantitative determination of niraparib and olaparib tumor distribution by mass spectrometry imaging, Int. J. Biol. Sci. 16 (2020) 1363–1375.

[53] S. Girod Fullana, H. Ternet, M. Freche, J.L. Lacout, F. Rodriguez, Controlled release properties and final macroporosity of a pectin microspheres-calcium phosphate composite bone cement, Acta Biomater. 6 (2010) 2294–2300.

[54] F. Munarin, P. Petrini, M.C. Tanzi, M.A. Barbosa, P.L. Granja, Biofunctional chemically modified pectin for cell delivery, Soft Matter 8 (2012) 4731–4739.

[55] F. Munarin, et al., Pectin-based injectable biomaterials for bone tissue engineering, Biomacromolecules 12 (2011) 568–577.

[56] S.C. Neves, et al., Biofunctionalized pectin hydrogels as 3D cellular microenvironments, J. Mater. Chem. B 3 (2015) 2096–2108.

[57] C.A. McKay, et al., An injectable, calcium responsive composite hydrogel for the treatment of acute spinal cord injury, ACS Appl. Mater. Interfaces 6 (2014) 1424–1438.

[58] S. Jäkel, L. Dimou, Glial cells and their function in the adult brain: A journey through the history of their ablation, Front. Cell. Neurosci. 11 (2017).

[59] S.C. Lange, L.K. Bak, H.S. Waagepetersen, A. Schousboe, M.D. Norenberg, Primary cultures of astrocytes: Their value in understanding astrocytes in health and disease, Neurochem. Res. 37 (2012) 2569–2588.

[60] S.A. Goldman, W.A. Pulsinelli, W.Y. Clarke, R.P. Kraig, F. Plum, The effects of extracellular acidosis on neurons and glia in vitro, J. Cereb. Blood Flow Metab. 9 (1989) 471–477.

[61] D.B. Hansen, N. Garrido-Comas, M. Salter, R. Fern, HCO-3-independent pH regulation in astrocytes in Situ is dominated by V-ATPase, J. Biol. Chem. 290 (2015) 8039–8047.

[62] N. Wattanakorn, et al., Pectin-based bioadhesive delivery of carbenoxolone sodium for aphthous ulcers in oral cavity, AAPS PharmSciTech 11 (2010) 743–751.

[63] Y.D. Sanzgiri, E.M. Topp, L. Benedetti, V.J. Stella, Evaluation of mucoadhesive properties of hyaluronic acid benzyl esters, Int. J. Pharm. 107 (1994) 91–97.

[64] P.A. Markov, et al., Mechanical properties, structure, bioadhesion, and biocompatibility of pectin hydrogels, J. Biomed. Mater. Res. Part A 105 (2017) 2572–2581.

[65] H.C. Shin, A.W.G. Alani, D.A. Rao, N.C. Rockich, G.S. Kwon, Multi-drug loaded polymeric micelles for simultaneous delivery of poorly soluble anticancer drugs, J. Control. Release 140 (2009) 294–300.

[66] R. Saadati, S. Dadashzadeh, Z. Abbasian, H. Soleimanjahi, Accelerated blood clearance of PEGylated PLGA nanoparticles following repeated injections: Effects of polymer dose, PEG coating, and encapsulated anticancer drug, Pharm. Res. 30 (2013) 985–995.

[67] M. Wu, et al., Olaparib nanoparticles potentiated radiosensitization effects on lung cancer, Int. J. Nanomedicine 13 (2018) 8461–8472.

[68] P. Kaushik, E. Priyadarshini, K. Rawat, P. Rajamani, H.B. Bohidar, pH responsive doxorubicin loaded zein nanoparticle crosslinked pectin hydrogel as effective site-specific anticancer substrates, Int. J. Biol. Macromol. 152 (2020) 1027–1037.

[69] B. Derjaguin, L. Landau, Theory of the stability of strongly charged lyophobic sols and of the adhesion of strongly charged particles in solutions of electrolytes, Prog. Surf. Sci. 43 (1993) 30–59.

[70] B. Derjaguin, A theory of interaction of particles in presence of electric double layers and the stability of lyophobe colloids and disperse systems, Prog. Surf. Sci. 43 (1993) 1–14.

[71] E.J.W. Verwey, Theory of the stability of lyophobic colloids, J. Phys. Colloid Chem. 51 (1947) 631–636.

[72] S.A. MacPherson, G.B. Webber, R. Moreno-Atanasio, Aggregation of nanoparticles in high ionic strength suspensions: Effect of Hamaker constant and particle concentration, in: Advanced Powder Technology, vol. 23, Elsevier, 2012, pp. 478–484.

[73] J. Hendriks, et al., Optimizing cell viability in droplet-based cell deposition, Sci. Rep. 5 (2015).

[74] Y. Jeong, et al., Sprayable adhesive nanotherapeutics: mussel-protein-based nanoparticles for highly efficient locoregional cancer therapy, ACS Nano 12 (2018) 8909–8919.

[75] R. Deitrich, S. Zimatkin, S. Pronko, Oxidation of ethanol in the brain and its consequences, Alcohol Res. Health 29 (2006) 266–273.

[76] V. Casañas-Sánchez, J.A. Pérez, D. Quinto-Alemany, M. Díaz, Sub-toxic ethanol exposure modulates gene expression and enzyme activity of antioxidant systems to provide neuroprotection in hippocampal HT22 cells, Front. Physiol. 7 (2016) 312.

[77] M.T. Cidade, et al., Injectable hydrogels based on pluronic/water systems filled with alginate microparticles for biomedical applications, Materials (Basel). 12 (2019).

[78] M.H. Turabee, T.H. Jeong, P. Ramalingam, J.H. Kang, Y.T. Ko, N, N, N-trimethyl chitosan embedded in situ Pluronic F127 hydrogel for the treatment of brain tumor, Carbohydr. Polym. 203 (2019) 302–309.

[79] P.M. Strappe, D.W. Hampton, B. Cachon-Gonzalez, J.W. Fawcett, A. Lever, Delivery of a lentiviral vector in a Pluronic F127 gel to cells of the central nervous system, Eur. J. Pharm. Biopharm. 61 (2005) 126–133.

[80] D.G. Angelescu, et al., Synthesis and association of Ag(0) nanoparticles in aqueous Pluronic F127 triblock copolymer solutions, Colloids Surf. A Physicochem. Eng. Asp. 394 (2012) 57–66.

[81] G. Gyulai, et al., Preparation and characterization of cationic pluronic for surface modification and functionalization of polymeric drug delivery nanoparticles, Express Polym. Lett. 10 (2016) 216–226.

[82] C. Dannert, B.T. Stokke, R.S. Dias, Nanoparticle-hydrogel composites: From molecular interactions to macroscopic behavior, Polymers (Basel). 11 (2019).